TÜBİTAK

Turkish Journal of Physics

http://journals.tubitak.gov.tr/physics/

Research Article

Turk J Phys
(2013) 37: 198 – 207

doi:10.3906/fiz-1206-14

Equilibrium shapes and deformations of some rare earth nuclei in cranked Nilsson–Strutinsky shell correction approach

Antony JOSEPH[1,*], **Kizhakkath Kalam GIRIJA**[2,3]
[1]Department of Physics, University of Calicut, 673635 Kerala, India
[2]Department of Physics, University of Calicut, 673635 Kerala, India
[3]Department of Physics, M.P.M.M.S.N. Trusts College, Shoranur, 679122 Kerala, India

Received: 23.06.2012 • **Accepted:** 10.09.2012 • **Published Online:** 19.06.2013 • **Printed:** 12.07.2013

Abstract: The nuclear potential energies of neutron-deficient even-even rare earth nuclei $^{150-160}Dy$, $^{150-160}Er$, $^{150-160}Yb$, $^{158,162,166-176}Hf$, $^{160,164-178}W$, and $^{162,166,170-180}Os$ are computed within the framework of the cranked Nilsson–Strutinsky shell correction method. The ground state potential energy surface diagrams of these nuclei are analysed in terms of quadrupole deformation and the triaxiality parameter. The nuclear shapes and deformations in the ground state are found to be functions of Z and N. Even though most of the isotopes in this region seem to be prolate in the ground state, oblate and triaxial shapes are also predicted for some isotopes. It is also found that the rare earth nuclei provide a platform for the study of phenomena such as nuclear shape changes and shape coexistence.

Key words: Cranked Nilsson–Strutinsky shell correction method, PES diagram, deformation, quadrupole deformation parameter, triaxiality, spin, ground state shape

1. Introduction

The atomic nucleus is a highly complicated quantum mechanical system consisting of many nucleons. It can adopt different configurations according to the interacting forces between the nucleons. The most significant forces are the short-ranged attractive nuclear force between nucleons and the long-ranged repulsive Coulomb force between protons. The shell effects and pairing correlation also contribute to the determination of nucleonic configuration. Depending on the configurations, the atomic nuclei exhibit spherical, quadrupole, and higher order multipole deformed shapes. It is also found that different shapes may coexist at the same spin and similar energies, which is considered to be the result of an interplay between a single particle and collective degrees of freedom [1],[2],[3],[4]. Hence, a mere spherical picture can not reflect the real nuclear structure.

Nuclei having spherical shape in their ground state (g.s) are few in number [2]. The deformed nuclei are classified as prolate, oblate, and triaxial. Prolate and oblate nuclei are axially symmetric. If the third axis of the nucleus is longer than the others, the nucleus is prolate, and if it is shorter, the nucleus is oblate. For triaxial nuclei, the 3 axes are different. In nature, prolate nuclei dominate over oblate ones [3]. It is found that 86% of the even-even nuclei are prolate in the ground state [5] and triaxial shapes are very rare for them. The effect of Coulomb repulsion between protons is to deform the nucleus into an elongated shape more than to a flattened shape. The difference in the volume element of the collective coordinates between prolate and oblate shapes is pointed out to be another reason for the prolate dominance over the oblate shape. The spin-orbit

*Correspondence: ajvar@rediffmail.com

potential (coupling) between nucleons plays a role in favouring a stable prolate shape for nuclei [5], [6]. The shell structure of nuclei is also responsible for the variety of shapes, depending on the position of the Fermi level between 2 closed shells [4]. The nuclear deformation is characterised by 2 collective parameters, the deformation parameter β or ε and the triaxiality γ. Positive and negative quadrupole deformations (β_2 or ε_2) correspond to prolate and oblate shapes, respectively. For $\gamma = 60^\circ, 0^\circ, -60^\circ$, and -120°, the nucleus is axially symmetric, and it is triaxial for all other γ values. $\gamma = 0^\circ$ and 60° represent prolate and oblate shapes, respectively.

Depending on the extent of deviation from spherical symmetry, the deformed nuclei fall into different groups. Nuclei with major to minor axes ratios around 1.3:1 are normally deformed and those with 1.5:1 are highly deformed. If the ratios are 2:1 and 3:1, the nuclei are superdeformed and hyperdeformed, respectively [2]. Nuclear deformation causes change in the potential energy of the nucleus. Thus, the nuclear potential energy surface (PES) can be exploited in the estimation of the shape evolution of nuclei with respect to angular momentum. At minimum potential energy, the nucleus will be in equilibrium. Hence, the deformation corresponding to the minimum potential energy decides the shape of the nucleus in its ground state.

The PES diagram is a 3D contour plot that indicates the variation of energy as a function of ε_2 and γ. Hence, it is an effective tool to predict the shape and deformation of nuclei in the g.s as well as in the excited states. It can also point out the possible superdeformed and hyperdeformed states of the nuclei. Stable deformed nuclei with $\beta_2 < 0.3$ are commonly found in the rare earth region [7], [8],[9]. These nuclei also provide a fertile region for the study of phenomena such as shape changes and shape coexistence [10]. Even though many attempts, both theoretical and experimental, have already been reported in the structural study in this region [1],[10],[11], [12],[13],[14],[15], the investigation of nuclear shapes and its evolution has been an outstanding problem in nuclear physics. In this paper, we make an attempt to investigate the g.s deformation and shapes of neutron-deficient even-even rare earth nuclei $^{150-160}Dy$, $^{150-160}Er$, $^{150-160}Yb$, $^{158,162,166-176}Hf$, $^{160,164-178}W$, and $^{162,166,170-180}Os$ exploring the cranked Nilsson–Strutinsky shell correction method and PES diagrams.

2. Theoretical formalisms

Nuclear deformation, which is the departure from spherical shape without density change, is expressed in terms of the shape parameters $\alpha_{\lambda\mu}$ and spherical harmonics $Y^{\mu}_{\lambda}(\theta,\phi)$ [16],[17],[18], as:

$$R(\theta,\phi) = R_0[1 + \sum_{\lambda\mu} \alpha_{\lambda\mu}(t) Y^{\mu}_{\lambda}(\theta,\phi)], \tag{1}$$

where R(θ,ϕ) is the distance of the nuclear surface at angles θ and ϕ from the centre and R_0 is the radius at spherical equilibrium. For each mode of order λ, μ has (2 λ+1) values, i.e. from $-\lambda$ to $+\lambda$. $\lambda = 1$ corresponds to dipole oscillation, $\lambda = 2$ to quadrupole oscillation, and $\lambda = 3$ to octupole oscillation. For quadrupole shapes,

$$R = R_0[1 + \sum_{\mu} \alpha_{2\mu} Y^{\mu}_{2}(\theta,\phi)]. \tag{2}$$

The deformation parameter β and the triaxiality γ are defined as [17]:

$$\alpha_{20} = \beta cos\gamma \tag{3}$$

and

$$\alpha_{22} = \alpha_{2-2} = \frac{1}{\sqrt{2}} \beta sin\gamma \tag{4}$$

so that

$$\sum |\alpha_{2\mu}|^2 = \beta^2, \tag{5}$$

since $\alpha_{21} = \alpha_{2-1} = 0$. ε is defined as $(R_{major} - R_{minor})/R_0$ [19] and the quadrupole deformations β_2 and ε_2 are related as: $\varepsilon_2 = 0.95\ \beta_2$ [19], [20].

For collective rotation of a nucleus [20],

$$H_{rot} = \frac{L^2}{2\jmath}, \tag{6}$$

where $\jmath$ is the moment of inertia and L is the collective angular momentum, which equals the total angular momentum I (total spin) in pure collective rotation. The rotational spectrum is then represented by [20]:

$$E_I = \frac{\hbar^2}{2\jmath} I(I+1). \tag{7}$$

The cranked Nilsson model accounts for the collective rotation of a deformed nucleus around an axis perpendicular to the symmetry axis. The nuclear potential energy is computed as a function of deformation and angular momentum. Here the rotation of an average field unsymmetric with respect to the rotation axis introduces a time dependence to the Schrodinger equation. Considering a rotating frame, with Z as the symmetry axis and X as the cranking axis, this may be reduced to a stationary equation [21]:

$$i\hbar \frac{\partial}{\partial t} \psi_{intr} = H^{\omega} \psi_{intr}, \tag{8}$$

where

$$H^{\omega} = H_{intr} - \hbar\omega I_x \tag{9}$$

is called the cranking Hamiltonian or Routhian. Here, the suffix *intr* stands for intrinsic, i.e. H_{intr} is the Hamiltonian and ψ_{intr} is the corresponding eigenvector in the rotating frame (body fixed frame, rotating with an angular frequency ω). I_x denotes the X component of total angular momentum. Since H^{ω} does not depend on time, the solution of the equation can be reduced to the eigenvalue problem of H^{ω}.The diagonalisation of the Hamiltonian gives the eigenvalues e_i^{ω} and the eigenvector ψ_i^{ω}. The single particle energies in the laboratory system and the single particle spin contributions m_i are obtained as [22]:

$$e_i = < \psi_i^{\omega} | h^0 | \psi_i^{\omega} > \tag{10}$$

and

$$m_i = < \psi_i^{\omega} | j_x | \psi_i^{\omega} >, \tag{11}$$

h^0 being the single particle Hamiltonian. The total single particle energy and spin are defined as:

$$E_{sp} = \sum_{occ} e_i = \sum_{occ} e_i^{\omega} + \hbar\omega \sum_{occ} m_i \tag{12}$$

$$I = \sum m_i. \tag{13}$$

Here, summation is over all occupied orbitals. The shell correction is given in such a way that [22]:

$$E_{shell}(I) = E_{sp}(I) - < E_{sp}(I) > . \tag{14}$$

Now, the total energy is dependent on I and $\bar{\varepsilon}$:

$$E_{tot}(\bar{\varepsilon}, I) = E_{Shell}(\bar{\varepsilon}, I) + E_{RLD}(\bar{\varepsilon}, I) \tag{15}$$

where E_{RLD} is the energy in the rotating liquid drop model[22],[23],[24] and

$$\bar{\varepsilon} = (\varepsilon, \gamma). \tag{16}$$

The constraint incompressibility of nuclear matter is taken into account by restricting a constant volume to the deformed nucleus. This is made possible by varying the cranking frequency $\omega_0(\varepsilon, \gamma)$ from its value at spherical shape ω_0^0 [22]. The moment of inertia is employed as done by Anuradha et al. [25]. The calculations are performed in a stretched coordinate system with the modified single particle oscillator potential [22], [26]:

$$h_0 = \frac{p^2}{2m} + \frac{1}{2}m(\omega_x^2 x^2 + \omega_y^2 y^2 + \omega_z^2 z^2) + Cl.s + D(l^2 - < l^2 >), \tag{17}$$

where C = – 2 $\kappa\hbar\omega_0$ and D = $-\kappa\mu\hbar\omega_0$, κ and μ being the Nilsson parameters. The values of κ and μ employed in the calculation are taken from Ref 22.

The 3 oscillator frequencies are given as [20], [22]:

$$\omega_x = \omega_0[1 - \frac{2}{3}\varepsilon cos(\gamma + \frac{2\pi}{3})] \tag{18}$$

$$\omega_y = \omega_0[1 - \frac{2}{3}\varepsilon cos(\gamma - \frac{2\pi}{3})] \tag{19}$$

$$\omega_z = \omega_0[1 - \frac{2}{3}\varepsilon cos\gamma], \tag{20}$$

so that

$$\omega_x\omega_y\omega_z = (\omega_0^0)^3. \tag{21}$$

Energy values corresponding to each combination of I, ω, and γ were then estimated.

3. Results and discussion

The total energy calculations are performed for the rare earth nuclei $^{150-160}Dy$, $^{150-160}Er$, $^{150-160}Yb$, $^{158,162,166-176}Hf$, $^{160,164-178}W$, and $^{162,166,170-180}Os$, in the spin range of 0–60 in steps of 10 units. The range of triaxiality parameter used is 0–60° and a frequency range of 0–1.5 MeV is employed. The quadrupole deformation parameter ε_2 is varied from 0 to 1. The major role of the deforming quadrupole force rather than the hexadecapole force in deciding the equilibrium state was well established in the studies of Baranger and Kumar [27]. Hence, the hexadecapole deformation ε_4 is not considered in these calculations.

The change in total energy with respect to the quadrupole deformation parameter ε_2 is illustrated in Figure 1 for ^{158}Er and ^{164}W (at $\gamma = 0$) for different spin values. In both cases, energy decreases initially with ε_2 and then increases, with a minimum at g.s ε_2. There is an appreciable change in energy with respect to ε_2 for ^{158}Er at all spin values, but ^{164}W shows a significant change only at low spins.

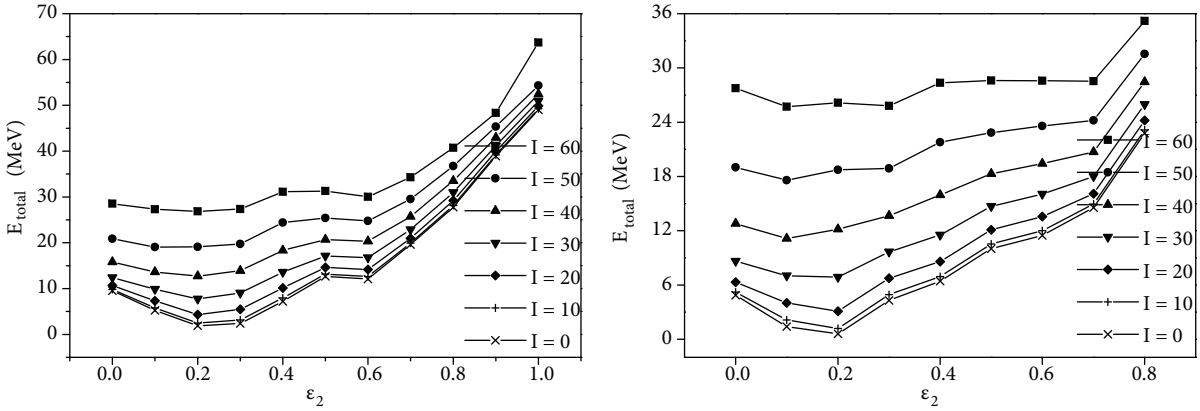

Figure 1. Total energy of ^{158}Er (left) and ^{164}W (right) as a function of quadrupole deformation ε_2 (at $\gamma = 0$).

Figure 2 indicates the variation in energy with respect to γ for ^{152}Dy, ^{158}Er, and ^{172}Os (at $\varepsilon_2 = 0.2$) for spins 0–60. In the first 2 cases, at low spins E_{tot} increases as γ changes from 0 to 60° (prolate to oblate), and at high spins it decreases as the nucleus makes an evolution from prolate ($\gamma = 0$) to oblate ($\gamma = 60°$). ^{172}Os shows an increase in energy as it evolves from prolate ($\gamma = 0$) to oblate ($\gamma = 60°$) shape in the entire range of spin 0–60.

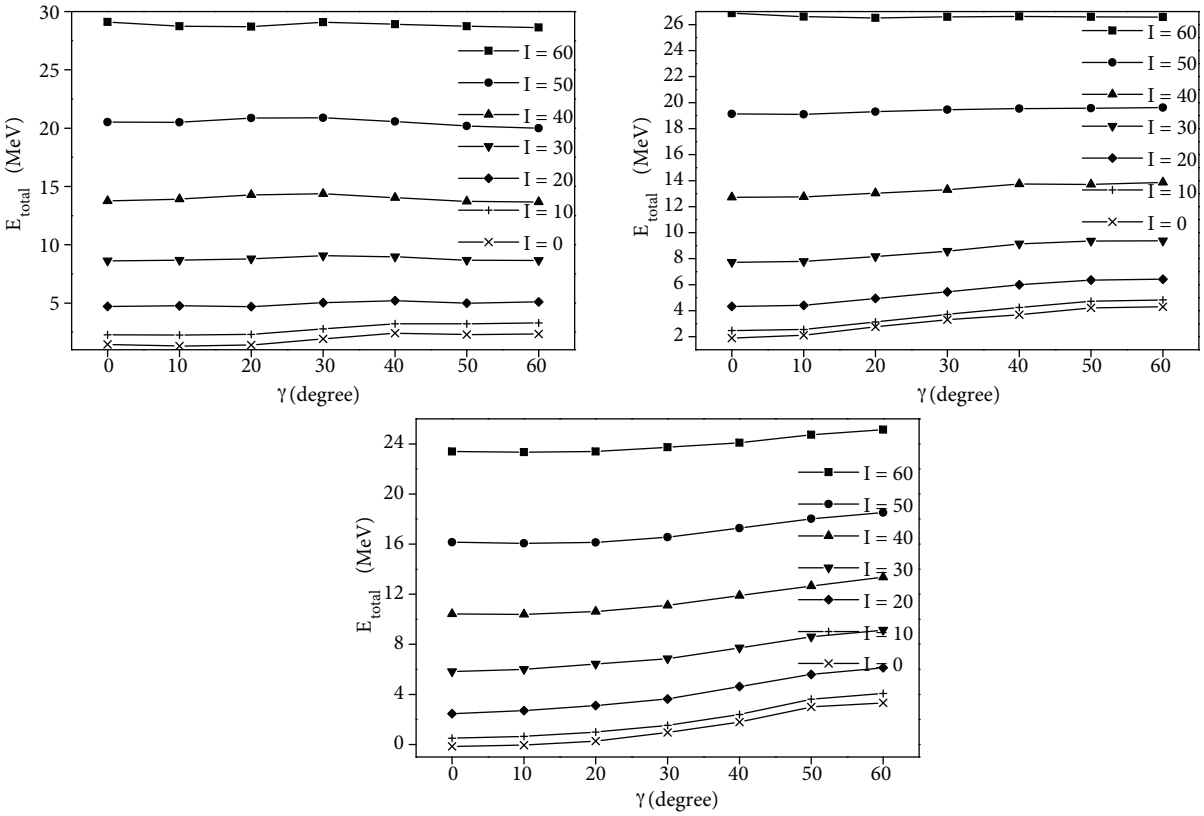

Figure 2. Total energy of ^{152}Dy (top left), ^{158}Er (top right), and ^{172}Os (bottom) as a function of triaxiality parameter γ (at $\varepsilon_2 = 0.2$).

From the PES diagrams, the g.s quadrupole deformations and equilibrium shapes of the selected isotopes are identified and are tabulated in Table 1. The calculated values are in agreement with the values from mass and deformation tables [28]. The g.s deformations were evaluated by Naik et al. [10] with nonrelativistic and relativistic Hartree–Fock approximations for some Hf, W, and Os isotopes in the same mass range. Lalazissis et al. [11] made a quantitative as well as qualitative estimation of g.s deformations of some Dy, Er, and Yb isotopes with the relativistic mean field theory. Our results are comparable with the findings of both of these groups. The available experimental values of g.s quadrupole deformations from atomic data and nuclear data tables [29] are also displayed in Table 1 and are in support of the calculated values. The experimental values of deformations quoted by Naik et al. [10] and Lalazissis et al. [11] in their works are also included in the same table. Our calculated values are in good agreement with these. The systematics of nuclear deformation for rare

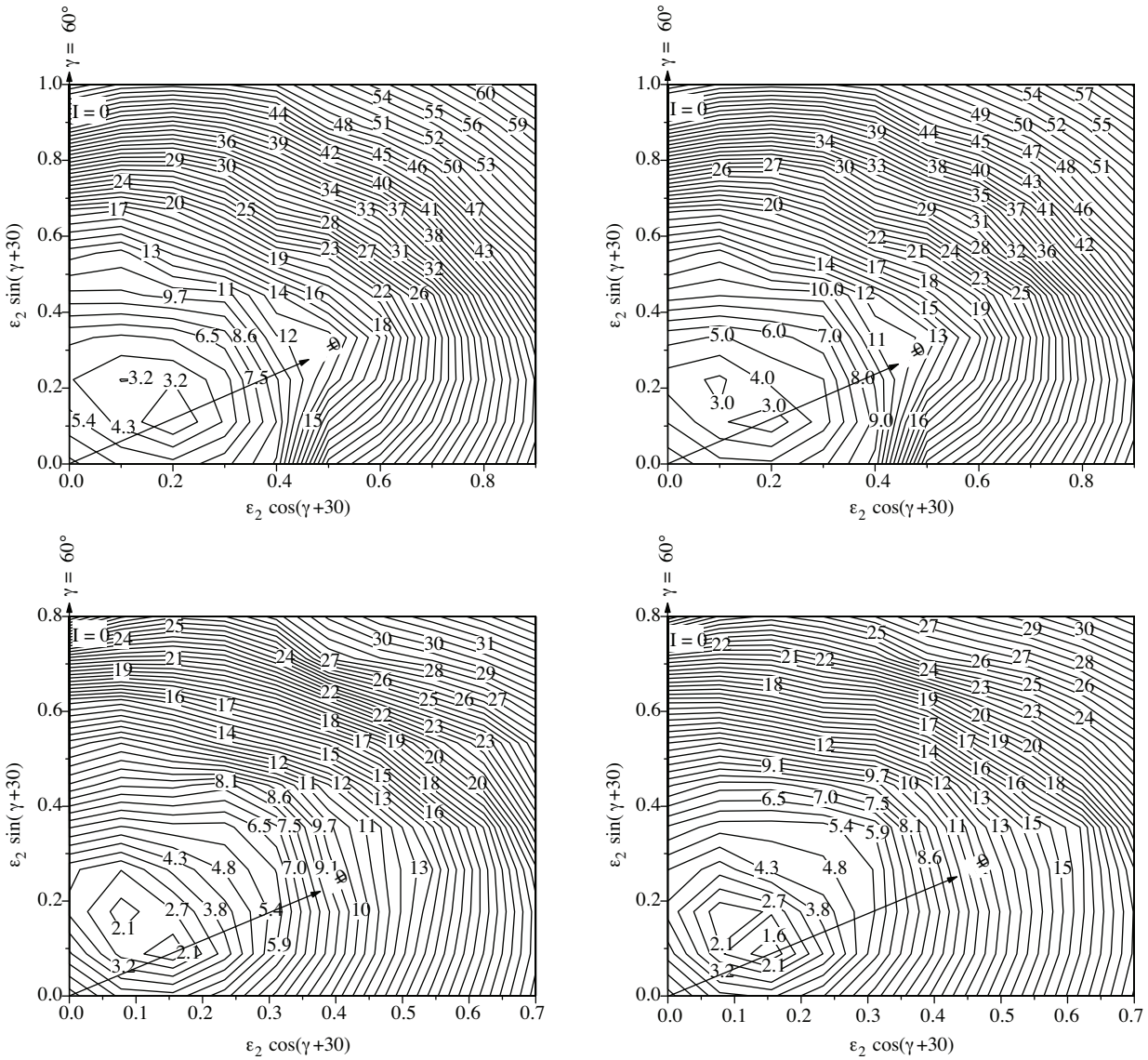

Figure 3. PES diagrams of $^{158}_{68}Er$ (top left), $^{160}_{70}Yb$ (top right), $^{162}_{72}Hf$ (bottom left), and $^{166}_{74}W$ (bottom right), showing the coexistence of prolate and triaxial minima.

Table 1. The computed ground state quadrupole deformations and shapes of selected nuclei.

	Ground state ε_2		Ground state β_2				Predicted
Nucleus	Cal.	From tables [28]	Cal.	Expt.[29]	Expt.[10]	Expt.[11]	g.s shape
$^{150}_{66}Dy$	–0.099	0	–0.104				Oblate
$^{152}_{66}Dy$	0.191	0.142	0.201	0.086		0.086	Prolate
$^{154}_{66}Dy$	0.225	0.192	0.237	0.237		0.237	Prolate
$^{156}_{66}Dy$	0.247	0.217	0.260	0.293		0.293	Prolate
$^{158}_{66}Dy$	0.260	0.242	0.274	0.326		0.326	Prolate
$^{160}_{66}Dy$	0.263	0.250	0.277	0.337		0.337	Prolate
$^{150}_{68}Er$	–0.089	–0.008	–0.094				Oblate
$^{152}_{68}Er$	–0.101	–0.017	–0.106				Oblate
$^{154}_{68}Er$	0.160	0.133	0.168				Oblate
$^{156}_{68}Er$	0.203	0.175	0.214	0.189		0.189	Prolate
$^{158}_{68}Er$	0.236	0.200	0.248	0.254		0.254	Prolate
	0.240		0.253				Triaxial
$^{160}_{68}Er$	0.254	0.233	0.267	0.303		0.303	Prolate
$^{150}_{70}Yb$	–0.138	–0.150	–0.145				Oblate
$^{152}_{70}Yb$	–0.077	0	–0.081				Oblate
$^{154}_{70}Yb$	–0.095	–0.008	–0.100				Oblate
$^{156}_{70}Yb$	0.142	0.117	0.150				Oblate
$^{158}_{70}Yb$	0.178	0.150	0.187	0.193		0.193	Triaxial
$^{160}_{70}Yb$	0.214	0.192	0.225	0.222		0.222	Prolate
	0.223		0.235				Triaxial
$^{158}_{72}Hf$	0.122	0.100	0.128				Triaxial
$^{162}_{72}Hf$	0.182	0.167	0.192				Prolate
	0.191		0.201				Triaxial
$^{166}_{72}Hf$	0.208	0.208	0.219	0.249	0.249		Triaxial
$^{168}_{72}Hf$	0.231	0.233	0.243	0.274	0.274		Triaxial
$^{170}_{72}Hf$	0.265	0.250	0.279	0.296	0.296		Triaxial
$^{172}_{72}Hf$	0.265	0.258	0.279	0.274	0.274		Triaxial
$^{174}_{72}Hf$	0.264	0.258	0.278	0.284	0.284		Triaxial
$^{176}_{72}Hf$	0.258	0.250	0.272	0.295	0.295		Triaxial
$^{160}_{74}W$	0.109	0.083	0.115				Triaxial
$^{164}_{74}W$	0.165	0.150	0.174				Prolate
$^{166}_{74}W$	0.177	0.167	0.186				Prolate
	0.189		0.199				Triaxial
$^{168}_{74}W$	0.191	0.192	0.201	0.232	0.232		Prolate
$^{170}_{74}W$	0.203	0.208	0.214	0.242	0.242		Prolate
$^{172}_{74}W$	0.251	0.233	0.264	0.308	0.309		Triaxial
$^{174}_{74}W$	0.245	0.242	0.258	0.251			Triaxial
$^{176}_{74}W$	0.233	0.242	0.245				Triaxial
$^{178}_{74}W$	0.231	0.242	0.243				Prolate
$^{162}_{76}Os$	0.094	0.042	0.099				Oblate
$^{166}_{76}Os$	0.137	0.125	0.144				Nearly prolate
$^{170}_{76}Os$	0.186	0.158	0.196				Prolate
$^{172}_{76}Os$	0.205	0.175	0.216	0.255			Prolate
$^{174}_{76}Os$	0.228	0.208	0.240	0.266			Prolate
$^{176}_{76}Os$	0.228	0.225	0.240				Prolate
$^{178}_{76}Os$	0.227	0.225	0.239				Prolate
$^{180}_{76}Os$	0.227	0.217	0.239	0.226			Prolate

earth nuclei were prepared by Tanaka et al. [12]. Since most of the isotopes that we considered are lighter than those that appeared in these systematics, a direct comparison is not made.

In most cases, we got one minimum. The isotopic chains of Dy, Er, and Os show a shape change from oblate to prolate as N increases. In addition, ^{158}Er possesses a triaxial yrast with $\varepsilon_2 = 0.240$, which is as equally deep as the prolate yrast (3.2 MeV). The isotopic chain Yb follows the oblate g.s minimum up to A = 156, whereas it is triaxial at A = 158. In ^{160}Yb, the competition between prolate and triaxial g.s minima with $\varepsilon_2 = 0.214$ and 0.223, respectively, and with same depth of 3 MeV is seen. All of the members in the Hf isotopic chain have a triaxial g.s minimum. In ^{162}Hf, the coexistence of a prolate ($\varepsilon_2 = 0.182$) yrast with the triaxial ($\varepsilon_2 = 0.191$) minimum with the same energy, 2.1 MeV, is also evident. W isotopes exhibit a shape change from triaxial to prolate, and then to triaxial and again to prolate as N changes from 86 to 104. Here also we could observe the coexistence of stable prolate ($\varepsilon_2 = 0.177$) and triaxial ($\varepsilon_2 = 0.189$) shapes at A = 166. Only in ^{166}W is the prolate minimum (1.6 MeV) deeper than the triaxial minimum (2.1 MeV). It is worth mentioning that the coexistence of prolate and triaxial shapes are predicted at N = 90, except for W (for which

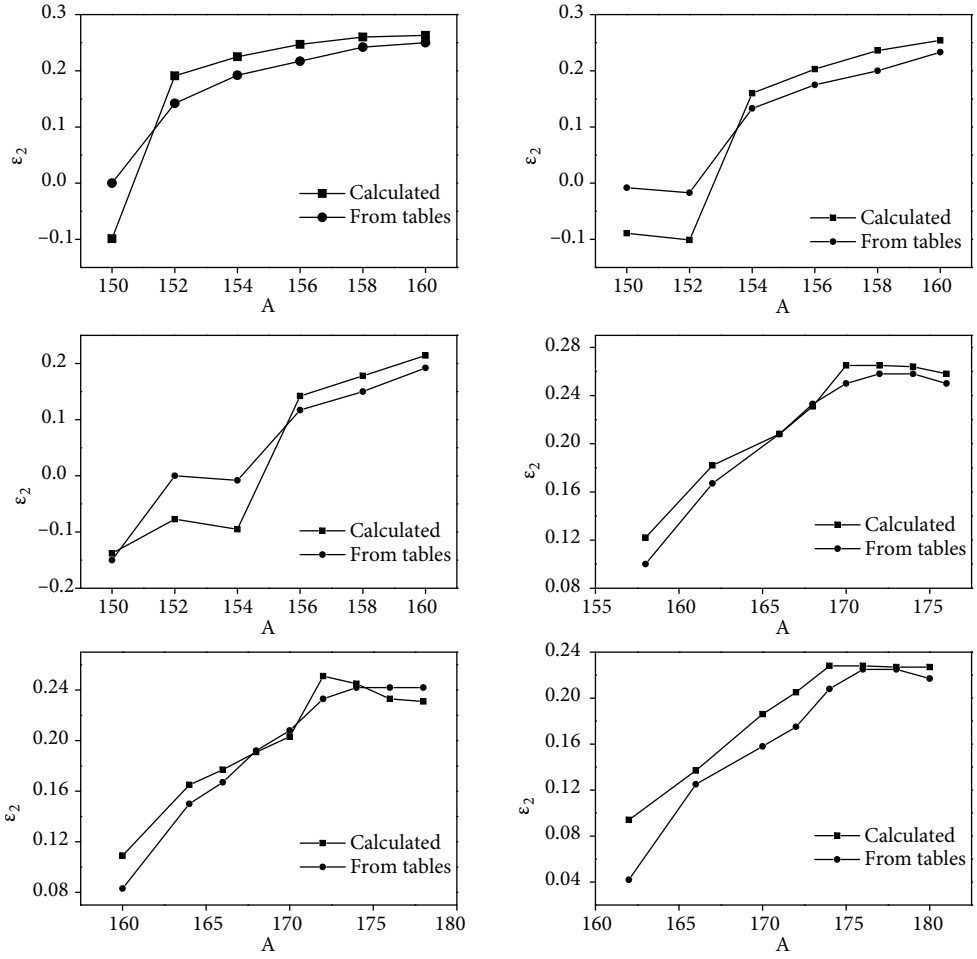

Figure 4. The ground state quadrupole deformations ε_2 (axial) of $_{66}Dy$ (top left), $_{68}Er$ (top right), $_{70}Yb$ (middle left), $_{72}Hf$ (middle right), $_{74}W$ (bottom left), and $_{76}Os$ (bottom right) isotopes as functions of mass number. Comparison is made with the values from deformation tables [28].

it is at N = 92). The coexistence of prolate and triaxial shapes in these nuclei are depicted in Figure 3 by the PES diagrams, which show that in an isotonic chain (only ^{158}Er, ^{160}Yb, and ^{162}Hf) as Z increases, the nuclei exhibit coexistence of prolate and triaxial shapes at a lower energy.

The g.s quadrupole deformations (axial) against mass number for the isotopic chains of Dy, Er, Yb, Hf, W, and Os are plotted in Figure 4. Since the experimental values do not depict the sign of deformation, these are not shown here. Such calculations were done by Anuradha et al. [25] for some odd Z nuclei in the range of $60 < Z < 80$. Here, the change in ε_2 with mass number in the case of Z = 67, 69, and 79 is in contradiction with what we obtained in the case of neighbouring even-even nuclei. This confirms the significance of proton number (odd or even) in fixing the g.s shape and deformation of nuclei. An analysis of Table 1 and Figure 4 reveals the mass number or N dependence of g.s quadrupole deformation. At N = 82, the magic number, g.s quadrupole deformation is minimum, which indicates an approach towards spherical shape for the nucleus. As N departs from 82, g.s quadrupole deformation increases. Around N = 100 (the middle of the closed shell), it is nearly constant and thereafter reduced. It is also found that the g.s quadrupole deformation decreases gradually with increasing proton number (Z) from the middle of the closed shell (Z = 66) towards the next magic number, 82, at a fixed neutron number (N), which is evident from Table 2 for N = 86 and 90. The same was verified by Robledo et al. [13] for N = 110–122 in Yb, Hf, W, Os, and Pt nuclei with the Gogny D1S interaction. This reiterates the dominant role of particle numbers and closed shell effects in deciding the g.s deformation.

Table 2. The computed ground state quadrupole deformations and shapes for different Z at constant neutron number.

Nucleus	Z	Ground state quadrupole deformation ε_2 and shape	
		For N = 86	For N = 90
Dy	66	0.191 Prolate	0.247 Prolate
Er	68	0.160 Oblate	0.236 Prolate 0.240 Triaxial
Yb	70	0.142 Oblate	0.214 Prolate 0.223 Triaxial
Hf	72	0.122 Triaxial	0.182 Prolate 0.191 Triaxial
W	74	0.109 Triaxial	0.165 Prolate
Os	76	0.094 Oblate	0.137 Prolate

4. Conclusions

The cranked Nilsson–Strutinsky shell correction method and PES diagrams were found to be powerful tools in the investigation of nuclear structure. Within this framework, the values of g.s quadrupole deformation in the well-established mass and deformation tables could be reproduced. It was also found that the calculated quadrupole deformations are comparable with the results of other models. The available experimental values of quadrupole deformation are also in support of our estimated quantities, which indicates the validity of the methodology that we used. The g.s shapes and deformations of nuclei are strongly dependent on Z and N. The major role played by closed shell effects is also revealed. Even though most of the nuclei possess a single g.s minimum, the coexistence of prolate and triaxial shapes is confirmed in the case of ^{158}Er, ^{160}Yb, ^{162}Hf, and ^{166}W isotopes. A region of coexistence around N = 90 is also predicted.

Acknowledgements

We benefited from discussions with Dr V. Ramasubramanian and Dr C. Anuradha, VIT University, Vellore, and we are grateful for their timely advice. One of the authors (KKG) expresses gratitude to UGC, Govt. of India, for the grant in aid under the FIP scheme.

References

[1] P.M. Walker, F.R. Xu and D.M. Cullen, *Phys. Rev.*, **C71**, (2005), 067303.

[2] R. Lucas, *Europhysics News*, **32**, (2001), 5.

[3] I. Maqbool, P. A. Ganai and J. A. Sheikh, *DAE-BRNS Proceedings of Int. Symp. on Nucl. Phys.*, **54**, (2009), 164.

[4] H. Sagawa, X. R. Zhou and X. Z. Zhang, *Phys. Rev.*, **C72**, (2005), 054311.

[5] N. Tajima and N. Suzuki, *Phys. Rev.*, **C64**, (2001), 037301.

[6] S. Takahara, N. Onishi, Y. R. Shimizu and N. Tajima, *Phys. Lett.*, **B702**, (2011), 429.

[7] P. Marmier and E. Sheldon, Physics of nuclei and particles, vol. 2 (Academic Press, New York. 1970) p. 1286.

[8] D. N. Poenaru and M. S. Ivascu, Particle emission from nuclei, ed. D. N. Poenaru and M. S. Ivascu, vol. 1, (CRC Press, Boca Raton, Florida. 1989) p. 17.

[9] J. Lilley, Nuclear physics - principles and applications, ed. D.J. Sandiford, F. Mandl and A.C. Phillips (John Wiley & Sons, New York. 2002) p. 59.

[10] Z. Naik, B. K. Sharma, T. K. Jha, P. Arumugam and S. K. Patra, *Pramana - J. Physics*, **62**, (2004), 827.

[11] G. A. Lalazissis, M. M. Sharma and P. Ring, *arXiv:nucl-th/9510058v1*, (1995).

[12] Y. Tanaka, R. M. Steffen, E. B. Shera, W. Reuter, M. V. Hoehn and J. D. Zumbro, *Phys. Rev.*, **C29**, (1984), 1830.

[13] L. M. Robledo, R. Rodriguez-Guzman and P. Sarriguren, *J. Phys. G: Nucl. Part. Phys.*, **36**, (2009), 115104.

[14] A. Aguilar, D. B. Campbell, K. Chandler, A. Pipidis, M. A. Riley, C. Teal, J. Simpson, D. J. Hartley, F. G. Kondev, R. M. Clark, M. Cromas, P. Fallon, I. Y. Lee, A. O. Macchiavelli and I. Ragnarsson, *Phys. Rev.*, **C77**, (2008), 021302(R).

[15] D. Sharma, S. Singh and A. Bharti, *Proceedings of the DAE Symposium on Nuclear Physics*, **56**, (2011), 388.

[16] S. S. M. Wong, Introductory nuclear physics (Prentice Hall of India, Pvt Ltd, New Delhi. 2007) p. 249.

[17] A. K. Jain and P. Arumugam, Mean field description of nuclei, ed. Y. K. Gambhir (Narosa Publishing House, New Delhi. 2006) p. 123.

[18] K. Heyde, Basic ideas and concepts in nuclear physics - an introductory approach, ed. D.F. Brewer (Overseas Press, India. 1998) p. 211.

[19] R. A. Sorensen, *Rev. of Modern Physics*, **45**, (1973), 353.

[20] S. G. Nilsson and I. Ragnarsson, Shapes and shells in nuclear structure (Cambridge University Press, Cambridge, UK. 1995) p. 125, 128, 182.

[21] M. J. A. de Voigt, J. Dudek, Z. Szymansky, *Rev. of Modern Physics*, **55**, (1983), 949.

[22] T. Bengtsson, I. Ragnarsson and S. Aberg, Computational nuclear physics I, ed. K. Langanke, J. A. Maruhn and S. E. Koonin (Springer-Verlag, Berlin. 1991) p. 52–55.

[23] W. D. Myers and W. J. Swiatecki, *Ark. Fys.*, **36**, (1967), 343.

[24] G. Vijayakumari and V. Ramasubramanian, *Int. Journal of Pure and Applied Sci.*, **2**, (2008), 36.

[25] C. A. Radha, V. Ramasubramanian and E. J. J. Samuel, *Turk. J. Phys.*, **34**, (2010), 159.

[26] H. Miri-Hakimabad and A. Kardan, *AIP Conference Proceedings-Carpathian Summer School of Physics-Exotic Nuclei and Nuclear/Particle/Astrophysics*, **1304**, (2010), 369.

[27] M. Baranger and K. Kumar, *Nucl. Phys.*, **62**, (1965), 113.

[28] P. Moller, J. R. Nix, W. D. Myers and W. J. Swiatecki, *At. Data Nucl. Data Tables*, **59**, (1995), 185.

[29] N. J. Stone, *At. Data Nucl. Data Tables*, **90**, (2005), 75.